# A Minimal Midzone Protein Module Controls Formation and Length of Antiparallel Microtubule Overlaps

Peter Bieling,[1,2] Ivo A. Telley,[1] and Thomas Surrey[1,*]
[1]Cell Biology and Biophysics Unit, European Molecular Biology Laboratory, Meyerhofstrasse 1, 69117 Heidelberg, Germany
[2]Present address: Department of Cellular and Molecular Pharmacology, University of California, San Francisco, San Francisco, CA 94158, USA
*Correspondence: surrey@embl.de
DOI 10.1016/j.cell.2010.06.033

## SUMMARY

During cell division, microtubules are arranged in a large bipolar structure, the mitotic spindle, to segregate the duplicated chromosomes. Antiparallel microtubule overlaps in the spindle center are essential for establishing bipolarity and maintaining spindle stability throughout mitosis. In anaphase, this antiparallel microtubule array is tightly bundled forming the midzone, which serves as a hub for the recruitment of proteins essential for late mitotic events. The molecular mechanism of midzone formation and the control of its size are not understood. Using an in vitro reconstitution approach, we show here that PRC1 autonomously bundles antiparallel microtubules and recruits Xklp1, a kinesin-4, selectively to overlapping antiparallel microtubules. The processive motor Xklp1 controls overlap size by overlap length-dependent microtubule growth inhibition. Our results mechanistically explain how the two conserved, essential midzone proteins PRC1 and Xklp1 cooperate to constitute a minimal protein module capable of dynamically organizing the core structure of the central anaphase spindle.

## INTRODUCTION

The various architectures adopted by the microtubule cytoskeleton are determined by distinct combinations of mechanochemical protein activities. How global properties of a complex cytoskeletal system, for instance characteristic shape and size, emerge from the local biochemical properties of the constituting molecules is an open question. During cell division, the microtubule cytoskeleton forms the mitotic spindle to segregate the duplicated set of chromosomes (Walczak and Heald, 2008). Spindles consist of two antiparallel arrays of microtubules that overlap in the spindle center, an organization that ensures spindle function. At anaphase onset, the central spindle reorganizes to form the midzone, a dense specialized array of antiparallel microtubules (Glotzer, 2009; Khmelinskii and Schiebel,

2008). The midzone size in metazoans is typically 2–3 $\mu$m in length (Mastronarde et al., 1993). Several proteins essential for spindle elongation, faithful chromosome segregation, and proper cytokinesis relocalize selectively to the central spindle as a consequence of changes in their phosphorylation patterns in anaphase: PRC1 (protein required for cytokinesis 1), kinesin-4, the centralspindlin complex (containing a kinesin-6), the chromosome passenger complex, and several other molecular motors, nonmotor microtubule-bundling proteins, and regulators (Glotzer, 2009). How the organization of the midzone is determined by the midzone proteins is, however, not understood.

The conserved vertebrate-bundling protein PRC1 (Jiang et al., 1998; Kurasawa et al., 2004; Mollinari et al., 2002; Zhu and Jiang, 2005) and its orthologs (Ase1 in yeasts [Loiodice et al., 2005; Schuyler et al., 2003], SPD-1 in *C. elegans* [Verbrugghe and White, 2004], Feo in *D. melanogaster* [Verni et al., 2004], and MAP65 in plants [Muller et al., 2004]) have emerged as key players for midzone formation. Ase1 in budding yeast has been proposed to be the core component of the spindle midzone. Genetic experiments have demonstrated that localization of all midzone proteins depends on Ase1, whose localization is independent of most other midzone proteins (Khmelinskii et al., 2007). Interestingly, fission yeast Ase1 has been shown to bind with some preference to antiparallel versus parallel microtubule bundles in vitro (Janson et al., 2007; Kapitein et al., 2008), indicating that recognition of antiparallel microtubules is an autonomous property of Ase1 in yeast.

In contrast to yeast, PRC1 in higher eukaryotes interacts with motor proteins of the kinesin-4 type. These chromokinesin motors relocalize to the central spindle in anaphase (Kurasawa et al., 2004; Kwon et al., 2004; Lee and Kim, 2004; Powers et al., 2004; Vernos et al., 1995; Zhu and Jiang, 2005). Correct localization of both PRC1 and kinesin-4 to the midzone depend on each other (Kurasawa et al., 2004; Zhu and Jiang, 2005; Zhu et al., 2005). However, whether kinesin-4 transports PRC1 to the midzone (Zhu and Jiang, 2005) or PRC1 selectively binds the central region of the anaphase spindle thereby recruiting kinesin-4 (Kurasawa et al., 2004) is presently unclear. Importantly, it is unknown how the size of the midzone is determined. Whereas absence of PRC1 results in complete loss of midzone microtubule bundles in mammalian cells (Kurasawa et al., 2004; Mollinari et al., 2002; Zhu and Jiang, 2005), absence of

kinesin-4 leads to increased anaphase spindle length (Kurasawa et al., 2004; Zhu and Jiang, 2005). Interestingly, a fragment of *Xenopus* kinesin-4 has been shown to decrease microtubule growth and shrinkage rates in vitro (Bringmann et al., 2004), an activity different from other regulators of microtubule dynamics (Howard and Hyman, 2007). Hence, kinesin-4 might contribute to midzone formation by regulating midzone microtubule dynamics. The minimal set of protein activities required for specific organizational features of the spindle midzone and the logic behind the combination of the required activities are, however, unknown.

We have developed an in vitro reconstitution approach to investigate the combinatorial action of purified full-length *Xenopus* kinesin-4 (Xklp1) and *Xenopus* PRC1 on microtubule organization and dynamics. We show that Xklp1 is recruited to antiparallel microtubule overlaps by PRC1, which autonomously discriminates between parallel and antiparallel microtubules with high selectivity. Xklp1 ensures the maintenance of microtubule overlap size by selectively inhibiting the growth of overlapping microtubules in a manner that is dependent on overlap length. Our results demonstrate that only two proteins are necessary and sufficient for the selective formation and for adaptable length control of antiparallel microtubule overlaps in vitro, as required for the formation of the midzone in vivo.

## RESULTS

### PRC1 Selectively Binds to Antiparallel Microtubule Overlaps with Nanomolar Affinity

We developed a fluorescence microscopy assay to visualize dynamic microtubule encounters in vitro. We attached short, Alexa 568- and biotin-labeled, stabilized microtubule seeds under flow to glass slides, which were functionalized with a NeutrAvidin-biotin-polyethylene glycol layer. The majority of the seeds aligned, and microtubules growing from these seeds in the presence of Alexa 568–tubulin occasionally encountered each other in a plus end-to-plus end configuration (Figure 1A). Multicolor time-lapse TIRF microscopy revealed that antiparallel microtubules connected in the presence of 5 nM purified PRC1–Alexa 647 as soon as their plus ends encountered, forming an antiparallel microtubule overlap (Figure 1B, Movie S1 available online). Interestingly, PRC1–Alexa 647 strongly accumulated in the growing antiparallel overlap region under conditions at which it did not localize significantly to individual microtubules or to parallel microtubule pairs (Figure 1C, Movie S1). This demonstrates that vertebrate PRC1 does not require an additional factor to selectively target antiparallel microtubule configurations. Autonomous binding to antiparallel microtubules, therefore, appears to be conserved between PRC1 orthologs from vertebrates and yeast (Janson et al., 2007).

The length of antiparallel microtubule overlaps increased linearly with time after the microtubule encounter (Figure 1D, top) indicating constant average overlap growth velocity. Overlap length as measured from plus end to plus end of the two antiparallel microtubules increased approximately twice as fast (4.9 ± 0.9 μm/min, mean ± standard deviation [SD]) as the length of single microtubules that were not part of an antiparallel microtubule pair (2.3 ± 0.3 μm/min) (Figure 1D, bottom), demonstrating

that the growth velocity of two microtubules of an antiparallel overlap is similar to that of individual microtubules and therefore not significantly affected by the strong accumulation of PRC1.

To investigate the mechanism by which vertebrate PRC1 specifically recognizes antiparallel overlaps, we quantified its affinity and selectivity of binding to distinct microtubule configurations. We measured the average fluorescence intensity of PRC1–Alexa 647 in antiparallel overlaps as a function of the PRC1–Alexa 647 concentration (Figure 1E, Figure S1A). PRC1 binding to antiparallel overlaps was strong and positively cooperative with a microscopic dissociation constant of 7.6 ± 0.4 nM (mean ± standard error of the mean [SEM]) and a Hill coefficient of 1.9 ± 0.1 (Figure 1E). Under standard imaging conditions, we did not detect any accumulation of PRC1 on individual microtubules or between parallel microtubules even at the highest PRC1 concentration used (31.5 nM) (Figure S1B). We estimate that PRC1 binds at least 28 times more strongly to antiparallel microtubule pairs than to individual or parallel microtubules (Extended Experimental Procedures), indicating considerably higher selectivity for antiparallel microtubules than previously reported for Ase1 from fission yeast (Janson et al., 2007).

To investigate the mechanism of this high binding selectivity, we imaged single PRC1 molecules at higher temporal resolution. Many binding events of individual PRC1–Alexa 647 molecules were detected in antiparallel overlaps (Figure 1F, right), whereas hardly any events were observed in parallel microtubule pairs (Figure 1F, left). Individual PRC1 molecules were not statically bound but diffused in antiparallel overlaps (Figures S1C and S1D). Despite the high affinity for antiparallel microtubules, turnover of PRC1 in antiparallel overlaps was fast with a single-molecule half-life of around 1 s (Figure 1G, Figure S1E). Therefore, selective binding to antiparallel microtubules is an intrinsic property of the individual PRC1 dimer and it is very dynamic. This appears to distinguish PRC1 from Ase1 whose moderate selectivity for antiparallel microtubule binding was suggested to be a consequence of the formation of slowly dissociating oligomers (Kapitein et al., 2008).

### Reconstitution of a Minimal Midzone with Stable Antiparallel Microtubule Overlaps In Vitro

We next tested the additional effect of *Xenopus* kinesin-4 Xklp1 on microtubule overlap formation. In the presence of both 5 nM purified PRC1–Alexa 647 and 15 nM purified Xklp1–GFP (Figure S2), antiparallel microtubules connected to each other as soon as their plus ends encountered, forming an antiparallel microtubule overlap that remarkably reached a constant size after awhile (Figure 2A, Movie S2, and Movie S3). PRC1–Alexa 647 and also Xklp1–GFP were observed to strongly accumulate selectively in antiparallel but not parallel overlap regions (Figure 2B, Movie S2). Xklp1 had only a minor positive effect on the amount of overlap-associated PRC1 (Figure 2C). In contrast, no Xklp1 was observed in the absence of PRC1 in antiparallel microtubule overlaps (Figures 2D–2F). Microtubules often failed to form a tight bundle in the presence of Xklp1 only (Movie S4), a behavior never observed when PRC1 was present.

These TIRF microscopy data indicate that Xklp1 interacts directly with PRC1, which we confirmed by pull-down experiments (Figure 2G, lane 2). Consequently, an N-terminal motor
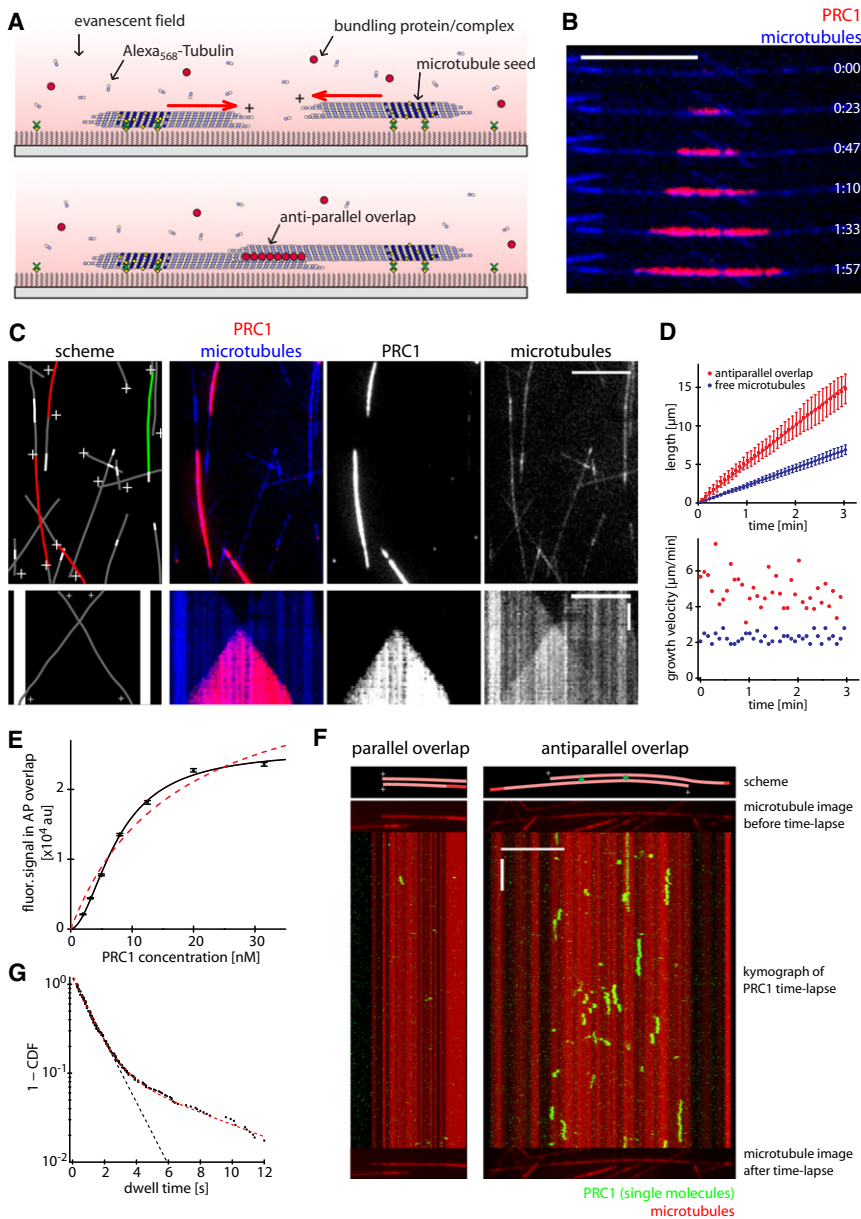
**Figure 1. PRC1 Preferentially Binds to and Diffuses in Antiparallel Microtubule Overlaps**

(A) Scheme of the experimental setup. Dynamic microtubules were grown in the presence of free Alexa 568-labeled tubulin (light blue) and fluorescently labeled midzone proteins (red) from stabilized microtubule seeds (dark blue) attached to a PEG-passivated glass surface by means of biotin–NeutrAvidin (yellow and green) links. Microtubules occasionally encountering each other in a plus end-to-plus end configuration forming an antiparallel microtubule overlap and fluorescently labeled midzone proteins were observed by multicolor time-lapse TIRF microscopy.

(B) Time sequence of overlaid TIRF microscopy images of PRC1–Alexa 647 (red, 5 nM) and a dynamic Alexa 568–microtubule pair (blue) forming an antiparallel overlap taken at the indicated times in min:s. The time-lapse was recorded at 1 frame per 4.67 s. Scale bar, 10 μm.

(C) TIRF images showing several microtubules growing from immobilized microtubule seeds, recorded 4–9 min after start of the experiment (top), and a kymograph (time-space plot) of a selected microtubule pair (bottom) in the presence of PRC1–Alexa 647. The kymograph begins ~1 min after start of the experiment. Left: schematic illustration of the microtubule configurations visible in the image and kymograph: microtubule segments (gray, plus ends labeled with "+") growing from seeds (white) form antiparallel (red) or parallel (green) overlaps. Parallel overlaps form from parallel seed bundles. Right: Overlaid and single-channel TIRF microscopy images and kymographs for PRC1–Alexa 647 and Alexa 568 microtubules as indicated. Concentrations and frame rate as in (B). Horizontal scale bars, 10 μm. Vertical scale bar, 1 min.

(D) Average length (top) and average instantaneous growth velocity (bottom) of antiparallel microtubule overlaps (red, n = 7) and of individual microtubules not part of a pair from the same experiment (blue, n = 14) forming in the presence of PRC1–Alexa 647 as a function of time. For antiparallel microtubule overlaps t = 0 is the moment of the plus end-to-plus end encounter. Error bars are standard deviation (SD). Concentrations are as in (B).

(E) Average fluorescence signal of PRC1–Alexa 647 bound to antiparallel microtubule overlaps plotted against the total PRC1–Alexa 647 concentration. Data (black points) were fitted either using the Hill equation (black, straight line) or a hyperbolic function (red, dotted line). At least a total of 100 μm of antiparallel overlap were evaluated per condition. Error bars are standard error of the mean (SEM).

(F) Single-molecule imaging of PRC1–Alexa 647 in a parallel (left) and an antiparallel (right) microtubule pair. Top: schematic representation of the pairs. Below: kymographs, positioned between TIRF microscopy images of microtubule overlaps before (top) and after (bottom) fast recording of individual PRC1–Alexa 647 molecules, showing the behavior of individual PRC1–Alexa 647 molecules (green). The PRC1–Alexa 647 concentration was 50 pM. Frame rate was 1 frame per 100 ms. Horizontal scale bar, 10 μm. Vertical scale bar, 5 s.

(G) Dwell time distribution plotted as 1 − cumulative distribution function (CDF) of individual PRC1–Alexa 647 molecules in antiparallel overlaps (black, n = 687). The red dashed curve is a biexponential fit with characteristic times $\tau_1 = 0.91 \pm 0.02$ s and $\tau_2 = 4.47 \pm 0.24$ s (mean ± 95% confidence interval [CI]), and relative amplitudes 87% $\tau_1$ and 13% $\tau_2$. The black dashed curve is a monoexponential fit. The mean bleaching time for Alexa 647 was $32.0 \pm 4.5$ s. Consequently $\tau_1$ is practically unaffected by bleaching and the corrected $\tau_2$ is 5.2 s.

See also Figure S1 and Movie S1.

fragment, Xklp506–GFP, that does not interact with PRC1 (Figure 2G, lane 3) failed to accumulate in antiparallel microtubule overlaps despite the presence of PRC1–Alexa 647, as observed by TIRF microscopy (Figure 2H, right). This shows that a direct interaction between Xklp1 and PRC1 is required for PRC1-dependent recruitment of Xklp1 to antiparallel microtubule overlaps.

The most striking observation in the presence of both midzone proteins was, however, that the growth of microtubule plus ends

being part of an antiparallel overlap slowed down until it ceased completely in all observed cases (n > 100) (Figure 2A, kymograph in 2B, 2H, left, Movie S2, Movie S3). The growth of overlap microtubules gradually stopped within about 1 min after the end-to-end encounter (Figure 2I, green). In contrast, individual microtubules not engaged in overlaps in the same experiment continued growing with constant velocity of 2.1 ± 0.3 (mean ± SD) μm/min (Figure 2I, blue). Inhibition of antiparallel microtubule overlap growth was a consequence of the simultaneous presence of PRC1 and full-length Xklp1. The presence of neither PRC1 alone (Figures 1B–1D) nor Xklp1 alone (Figure 2F) had a significant effect on microtubule growth in antiparallel overlaps. Hence, stable antiparallel overlaps with a constant size of several micrometers formed only in the presence of both midzone proteins (Figures 2A, 2B, and 2I; Movie S3). Such antiparallel microtubule overlaps maintained a constant size over long periods of time despite the complete inhibition of microtubule growth. This is remarkable, given that slowdown of microtubule growth usually results in frequent transitions to microtubule depolymerization (catastrophes) (Arnal et al., 2004; Janson et al., 2003; Walker et al., 1988).

Our results show that a "minimal midzone" can be reconstituted in vitro with dynamic microtubules and two proteins only: PRC1 is necessary and sufficient to recognize and bundle antiparallel microtubules. Xklp1 alone does not bind to antiparallel overlaps but is instead recruited by overlap-associated PRC1. This recruitment results in local inhibition of microtubule growth without causing microtubule depolymerization, leading to antiparallel microtubule overlaps of constant size.

## Xklp1 Inhibits Turnover of Tubulin at the Growing Microtubule End

To better understand how Xklp1 affects microtubule dynamics, we measured the effect of varying concentrations of Xklp1 alone on the dynamics of individual microtubules. Similar to an N-terminal fragment of Xklp1 (Bringmann et al., 2004), full-length Xklp1 alone reduced the growth velocity of microtubule plus ends in a concentration-dependent manner (Figures 3A and 3B). This effect could only be observed at Xklp1 concentrations of several hundred nanomolar, well above the Xklp1 concentrations in the lower nanomolar range that lead to inhibition of microtubule growth in antiparallel overlaps in the presence of PRC1. Interestingly, the catastrophe frequency remained very low at increasing Xklp1 concentrations (Figure 3C), despite the strong reduction in microtubule growth velocity, which is expected to lead to more frequent catastrophes (Arnal et al., 2004; Janson et al., 2003; Walker et al., 1988). The effect of Xklp1 on the catastrophe frequency is more evident when comparing microtubules growing with similar velocities (Figure 3D). The catastrophe frequencies of microtubules in the presence of Xklp1, plotted as a function of their growth velocities (Figure 3D, red), are significantly lower than those of microtubules growing at similar velocities in the absence of Xklp1 at reduced tubulin concentrations (Figure 3D, blue). This shows that Xklp1 inhibits catastrophes, explaining why local inhibition of microtubule growth by PRC1-recruited Xklp1 in antiparallel microtubule pairs (Figures 2A, 2B, and 2I) does not result in destabilization of the overlap.

To gain a better understanding of the effect of Xklp1 on the microtubule catastrophe frequency, we measured the microtubule growth velocity at different tubulin concentrations with and without 300 nM Xklp1 (Figure 3E). This allowed us to determine the association and dissociation rate constants of guanosine-5′-triphosphate (GTP)-tubulin at the growing plus end (Drechsel et al., 1992; Walker et al., 1988). We found that 300 nM Xklp1 reduced the on-rate of GTP-tubulin by a factor of about two and the off-rate by a factor of around three (Figure 3F). This shows that Xklp1 has the unique property of making microtubules less dynamic by reducing the overall turnover of GTP-tubulin at growing microtubule ends, distinguishing it from other known mitotic regulators of microtubule dynamics (Brouhard et al., 2008; Helenius et al., 2006; Varga et al., 2006).

## Dynamic Control of Antiparallel Microtubule Overlap Length

To investigate how the inhibitory effect of Xklp1 on tubulin turnover affects the length of antiparallel microtubule overlaps in the presence of PRC1, we varied the Xklp1:PRC1 ratio in antiparallel microtubule encounter experiments, leaving the PRC1 concentration constant (Figure 4A, Movie S5). At Xklp1:PRC1 ratios lower than 1, microtubule plus-end growth persisted over long times (>10 min) after formation of an antiparallel overlap, albeit at greatly reduced speeds as compared to microtubules that were not part of an overlap (Movie S5). At Xklp1:PRC1 ratios ≥1, microtubule plus ends within the antiparallel overlap stopped growing soon after their initial encounter leading to stable antiparallel overlaps with a distinct characteristic steady-state length for each Xklp1:PRC1 ratio (Figure 4B). The average steady-state overlap length decreased with increasing Xklp1 concentration, ranging from 4.2 μm to 1.2 μm for ratios from 1 to 20, respectively (Figure 4B). Thus the concentration of Xklp1 determines the steady-state length of the antiparallel microtubule overlap.

Next, we investigated whether the steady-state overlap lengths could reversibly respond to changes in the Xklp1 concentration (Figure 4C). We preformed short overlaps at high Xklp1:PRC1 ratios, followed by reduction of the Xklp1 concentration, keeping the PRC1 and tubulin concentrations constant. Strikingly, we observed that microtubules of short preformed overlaps started to grow again until they had reached the length characteristic for the new Xklp1:PRC1 ratio (Figures 4C–4E, Movie S6). These results demonstrate that the Xklp1:PRC1 ratio can dynamically control the steady-state overlap length.

Why do higher Xklp1:PRC1 ratios result in shorter antiparallel overlaps? The major contribution of Xklp1 in determining overlap length could be either its inhibitory effect on microtubule growth or, alternatively, a consequence of Xklp1 sliding apart antiparallel microtubules, similar to kinesin-5 (Kapitein et al., 2005). Indeed, we observed that microtubules engaged in antiparallel overlaps frequently buckled over time (Figure S3A), indicative of plus-end-directed microtubule sliding. The average sliding length (Extended Experimental Procedures) was, however, in all cases short as compared to the overlap length at steady state (Figure 4B). A plot of the individual sliding lengths of all microtubule pairs against their individual overlap length also did not reveal any correlation (Figure S3B). Therefore, antiparallel microtubule sliding does not significantly contribute here to overlap length control.
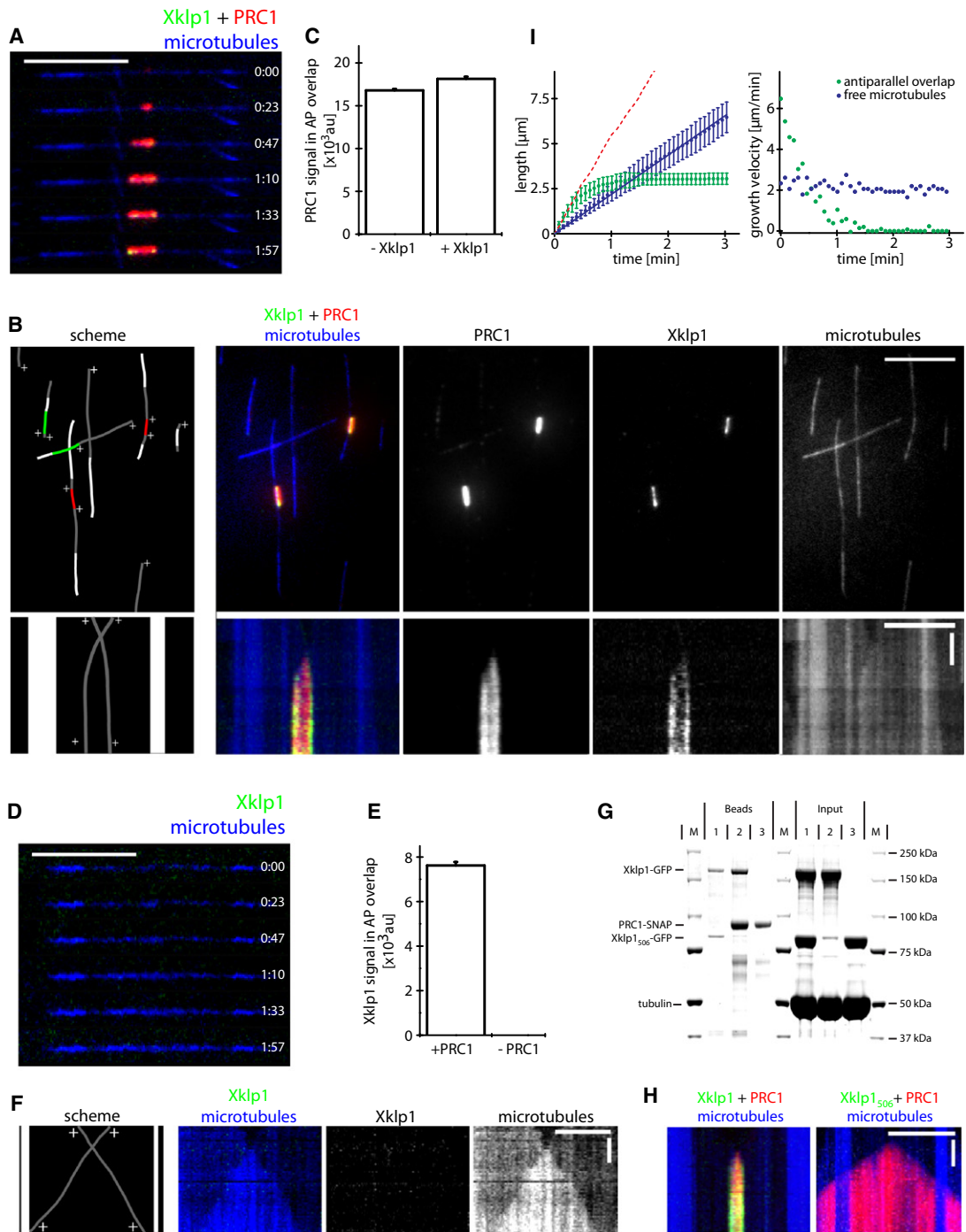
**Figure 2. A Minimal Protein System Forms Stable Antiparallel Overlaps In Vitro**

(A) Time sequence of overlaid TIRF microscopy images of PRC1–Alexa 647 (red, 5 nM) and Xklp1–GFP (green, 15 nM) in a dynamic Alexa 568-labeled microtubule pair (blue) forming an antiparallel overlap at the indicated times in min:s.

(B) TIRF images, recorded 4–9 min after the start of the experiment, showing several microtubules growing from immobilized microtubule seeds (top) and a kymograph of a selected microtubule pair (bottom). Left: schematic illustration of the microtubule configurations. Color coding as in Figure 1C. Right: overlaid and single-channel TIRF microscopy images and kymographs for PRC1–Alexa 647, Xklp1–GFP, and Alexa 568 microtubules as indicated. Concentrations as in (A).

(C) Average fluorescence intensity signal of PRC1–Alexa 647 bound to antiparallel microtubule overlaps in the presence (n = 45 overlaps) or absence (n = 18 overlaps) of Xklp1–GFP, obtained from intensity line scans. Error bars are SEM.

(D) Time sequence of overlaid TIRF images of 15 nM Xklp1–GFP (green) and a dynamic Alexa 568-microtubule pair (blue) forming an antiparallel overlap taken at the indicated times in min:s.
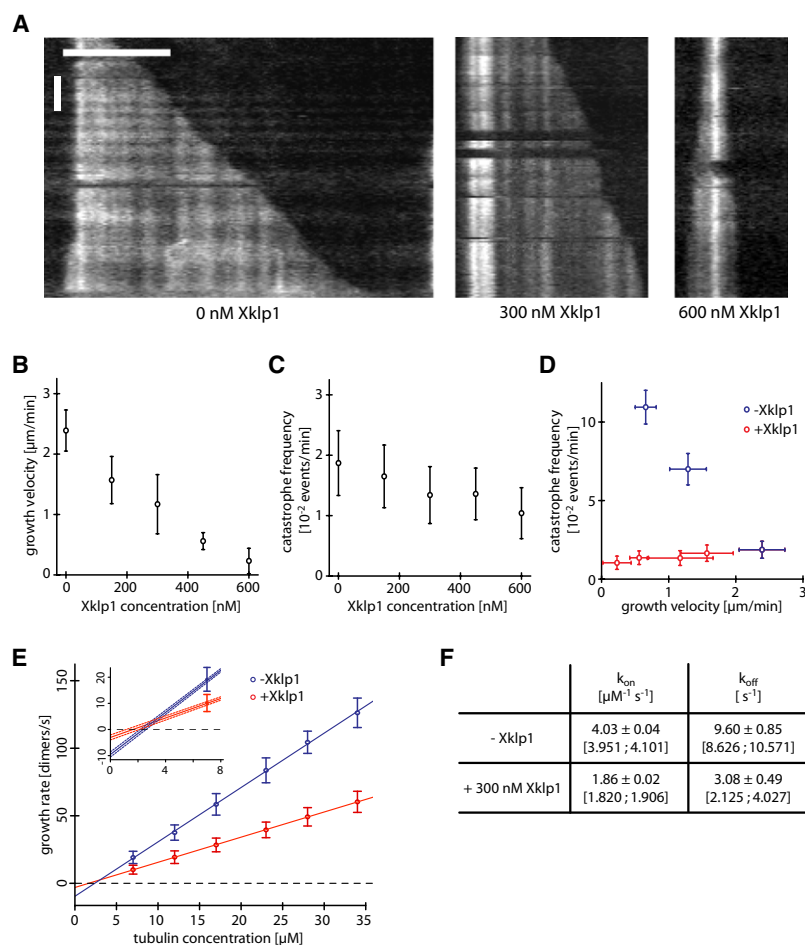
**Figure 3. Xklp1 Inhibits Turnover of Tubulin at the Growing Microtubule End**

(A) Representative kymographs of Alexa 568-labeled microtubules growing in the absence or presence of Xklp1–GFP (not shown) at the indicated concentrations. Concentration of soluble tubulin is 17.5 μM. The frame rate was 1 frame per 3 s. Horizontal scale bar, 10 μm. Vertical scale bar, 1 min.

(B) Average microtubule growth velocity and (C) catastrophe frequency plotted against the total Xklp1–GFP concentration. Sixty microtubules from two independent experiments were analyzed per condition.

(D) Catastrophe frequency as a function of microtubule growth velocity. Red data points are from experiments with 17.5 μM tubulin and varying Xklp1–GFP concentrations, as shown in (B) and (C). Blue data points are from experiments with varying tubulin concentrations (7, 12, and 17.5 μM) in the absence of Xklp1–GFP.

(E) Average growth rate in the absence (blue circles) or in the presence of 300 nM Xklp1–GFP (red circles) as a function of total tubulin concentration. A multiple linear regression model with a categorical factor $g$ (+Xklp1: $g = 0$, −Xklp1: $g = 1$) revealed that both the abscissa and the slope were significantly different ($p < 0.001$, see Experimental Procedures). The resulting regression lines represent $v_g = k_{on} c − k_{off}$ with the net assembly rate $v_g$ in tubulin dimers per second and the time constants for association $k_{on}$ in $s^{-1} μM^{-1}$ and dissociation $k_{off}$ in $s^{-1}$ of GTP-tubulin at the growing microtubule end. Inset: regression lines and their 95% confidence intervals (dashed) at the origin, showing that not only $k_{on}$ (slope) but also $k_{off}$ (intersection with abscissa) is different for the two conditions. 185 to 210 microtubules from two independent experiments were analyzed for each tubulin concentration per condition.

(F) Values for $k_{on}$ and $k_{off}$ (mean ± SEM, with 95% confidence in brackets) as obtained from fits in (E).

Error bars in (B)–(E) are SD.

## Xklp1 Is a Processive Motor

To elucidate the mechanism by which Xklp1 sets the size of antiparallel microtubule overlaps, we inspected the behavior of the motor more closely. Occasionally, antiparallel overlaps formed by lateral encounters between one microtubule end and one microtubule segment distant from the growing end (Figure 5A). In such cases, Xklp1–GFP loaded onto the overlap region by PRC1 also accumulated at the plus end of the microtubule extending beyond the overlap (Figure 5A). Interestingly, accumulation of Xklp1 at these free microtubule ends also resulted in inhibition of microtubule growth (Movie S7). This suggests that (1) it is the plus-end-associated fraction of Xklp1 that inhibits microtubule growth and (2) Xklp1 can target the plus end by means of processive motility over considerable distances. This is surprising, given that an N-terminal fragment of Xklp1 has been proposed to be at most weakly processive based on enzymatic activity assays (Bringmann et al., 2004).

(E) Average fluorescence intensity signal of Xklp1–GFP bound to the antiparallel microtubule overlap in the presence (n = 42 overlaps) or absence of PRC1–Alexa 647, as obtained from intensity line scans. Error bars are SEM.

(F) Kymograph of the microtubule pair shown in (D). Color code as in (B).

(G) Pull-down of Xklp1 by PRC1–SNAP immobilized on beads. Coomassie-stained SDS-gel shows fractions bound to the beads after incubation with different input solutions. Lanes 1: negative control with beads lacking PRC1–SNAP incubated with a mixture of 2 μM full-length Xklp1–GFP, 2 μM truncated Xklp1$_{506}$–GFP, and 5 μM soluble tubulin. Only weak nonspecific binding of the two Xklp1 proteins is seen. Lanes 2 and 3: beads with immobilized PRC1–SNAP incubated with either 2 μM full-length Xklp1–GFP (lanes 2) or truncated 2 μM Xklp1$_{506}$–GFP (lanes 3) in the presence of 5 μM soluble tubulin.

(H) Representative kymographs of antiparallel microtubule overlaps (blue) in the presence of PRC1–Alexa 647 (red, 5 nM) and either full-length Xklp1–GFP (green, 15 nM) (left) or truncated Xklp1$_{506}$–GFP (green, 15 nM) (right).

(I) Average length (left) and average instantaneous growth velocity (right) of antiparallel overlaps (green, n = 9) and individual microtubules that are not part of a pair from the same experiment (blue, n = 18) formed in the presence of PRC1 and full-length Xklp1 as a function of time (conditions as in A and B). For comparison, the length of microtubule overlaps formed in the presence of only PRC1 (from Figure 1D) is shown (red dashed line). t = 0 is the moment of plus end-to-plus end encounter. Error bars are SD. Concentrations are as in (A). Horizontal scale bars are 10 μm. Vertical scale bars are 1 min. The frame rate for all time-lapse movies was 1 frame per 4.67 s. Kymographs start ∼1 min after the start of the experiment.

See also Figure S2 and Movie S2, Movie S3, and Movie S4.
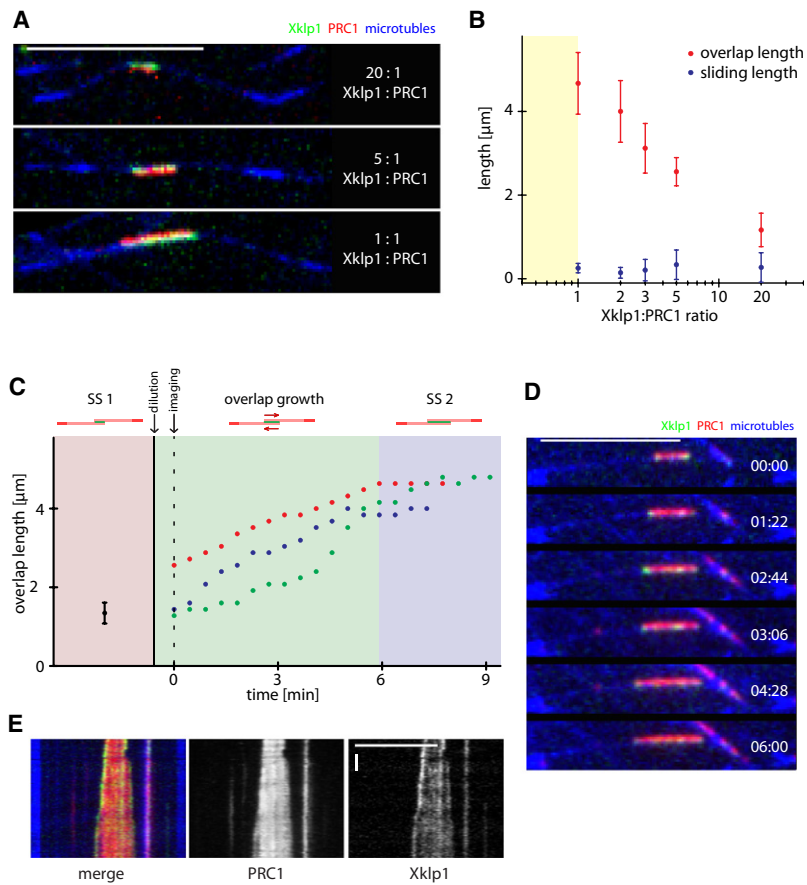
**Figure 4. Dynamic Control of Antiparallel Overlap Length**

(A) Representative triple-channel TIRF microscopy images of PRC1–Alexa 647 (red, 5 nM) and Xklp1–GFP (green, 100, 25, and 5 nM) at PRC1:Xklp1 ratios as indicated in a dynamic Alexa 568–microtubule pair (blue) forming an antiparallel overlap. Images were recorded 7–12 min after start of the experiment. Scale bar, 10 $\mu$m.

(B) Average overlap length (red) or average sliding length (blue) as a function of the Xklp1:PRC1 ratio. Error bars are SD. Overlap lengths and sliding lengths were measured for at least 15 overlaps from at least three experiments per condition after steady state had been reached. Yellow shading indicates the regime where no steady-state length was established.

(C) Reversibility experiment: Antiparallel microtubule overlaps were allowed to form at 100 nM Xklp1–GFP and 5 nM PRC1–Alexa 647 (Xklp1:PRC1 ratio 20:1) and to reach their steady-state length (black dot with SD bars in red area). Subsequently, Xklp1–GFP was diluted to 5 nM keeping the PRC1–Alexa 647 and tubulin concentrations constant (new Xklp1:PRC1 ratio 1:1, details in Experimental Procedures). Quantification of overlap lengths versus time for three examples (dark green, blue, and red dots in green area) shows that after ~6 min the overlaps reach a new steady-state length characteristic for the new, lower Xklp1 concentration (purple area).

(D) Example time series of overlaid triple-channel TIRF microscopy images at the indicated times (min:s) after Xklp1–GFP dilution and (E) corresponding kymographs showing a representative growing overlap. The frame rate was 1 frame per 4.67 s. Colors and horizontal scale bar as in (A). Vertical scale bar, 1 min. See also Figure S3 and Movie S5 and Movie S6.

We therefore imaged single molecules of full-length Xklp1–GFP on stabilized, individual microtubules in the absence of PRC1. We observed that at low ionic strength Xklp1–GFP dimers indeed moved processively (Figure 5B) with an average run length of 1.2 $\mu$m (Figure 5C) and an average velocity of 0.8 $\mu$m/s (Figure 5F, red). Reduction in ionic strength was necessary because binding of Xklp1 to individual microtubules was very weak. Processivity was an intrinsic property of the dimerized motor domain, as demonstrated by imaging a GFP-labeled motor fragment (Figures 5D–5G). Run length (0.9 $\mu$m, Figure 5E) and velocity (0.9 $\mu$m/s, Figure 5F, black) of Xklp1$_{506}$–GFP were in a similar range as the values for the full-length motor. The longer dwell times of the full-length motor (Figure S4A) are probably a consequence of a secondary microtubule-binding site (Figure S4B). These results demonstrate that Xklp1 is a processive motor, suggesting that it might measure the overlap length by processive movement.

## Xklp1 Determines Overlap Length by a Processive Overlap Exploration Mechanism

To test the hypothetical mechanism of processive overlap length measurement, we imaged single full-length Xklp1–GFP molecules (500 pM) in the presence of excess PRC1–Alexa 647 (5 nM) in dynamic antiparallel microtubule pairs at high time resolution. Strikingly, Xklp1–GFP was very mobile in PRC1-containing antiparallel overlaps. Xklp1–GFP showed processive movement often abruptly changing direction, indicating a transition from one

to the other microtubule of the pair (Figure 6A, left, Figure S5A, Movie S8). This highly mobile behavior of the motor was very different from that of single PRC1–Alexa 647 molecules (5 pM) in the presence of excess PRC1–Alexa 488 (5 nM) in the overlap, which only diffused for very short distances (Figure 6A, right). The dwell time distribution of Xklp1–GFP in PRC1-containing antiparallel overlaps was roughly exponential (Figure 6B, black dots) with a calculated average dwell time of ~5.9 s (dashed red line). This demonstrates that Xklp1 dwells longer in a PRC1-decorated antiparallel overlap as compared to on individual microtubules in the absence of PRC1 at low ionic strength (Figure 6B, gray circles), and also longer than the individual PRC1 molecules in the antiparallel overlap (Figure 6B, blue dots). This shows that PRC1 increases the residence time of Xklp1 in the overlap probably by offering additional binding sites. Mean squared displacement (MSD) analysis confirmed that Xklp1 was very mobile in PRC1-containing overlaps (Figure 6C, black dots), in contrast to slowly diffusing PRC1 molecules (Figure 6C, blue dots; Figure S1C). However, Xklp1 explored shorter distances in PRC1-containing overlaps than on individual microtubules in the absence of PRC1 under low ionic strength conditions (Figure 6C, gray dots). The MSD curve of Xklp1 in antiparallel overlaps could be well described using a "persistent random walk" model (Figure 6C, dashed red line, Extended Experimental Procedures) (Othmer et al., 1988; Tranquillo and Lauffenburger, 1987). A fit to the data yielded a characteristic persistence time between
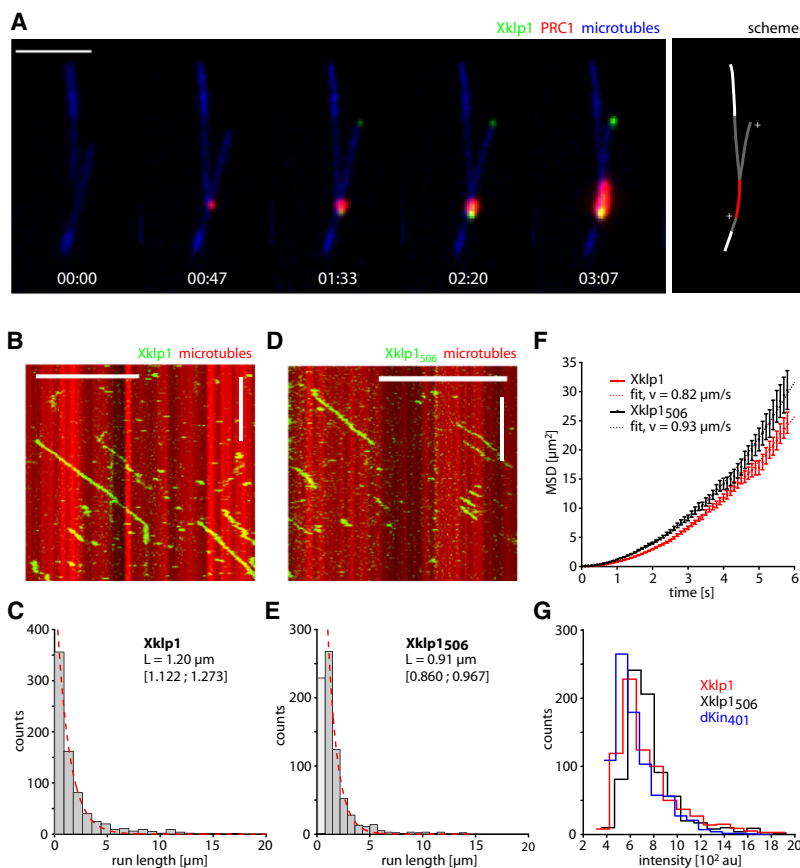
**Figure 5. Xklp1 Is a Processive Motor**

(A) Time sequence (min:s) of multichannel TIRF microscopy images of PRC1–Alexa 647 (red, 5 nM) and Xklp1–GFP (green, 15 nM) in a dynamic Alexa 568-labeled microtubule pair (blue) forming an antiparallel overlap by a lateral encounter between one microtubule plus end and one microtubule segment distant from its growing end, as illustrated in the scheme (right). Scale bar, 5 μm.

(B) Representative kymograph of individual full-length Xklp1–GFP dimers (green, 2.5 nM) on an individual stabilized microtubule (red) at low ionic strength (see Extended Experimental Procedures) imaged at high time resolution (10 frames/s). Horizontal scale bars, 10 μm. Vertical scale bar, 5 s.

(C) Histogram of the run length distribution of full-length Xklp1–GFP with a monoexponential fit (red dashed); mean run length was 1.20 μm (95% CI in brackets).

(D) Representative kymograph of individual Xklp1$_{506}$–GFP dimers (green, 20 nM) on an individual taxol-stabilized microtubule (red) at very low ionic strength conditions (see Extended Experimental Procedures). Imaging and bars as in (B).

(E) Histogram of the run length distribution of Xklp1$_{506}$–GFP with a monoexponential fit (red dashed); mean run length was 0.91 μm (95% CI in brackets).

(F) Mean squared displacement (MSD) curve of full-length Xklp1–GFP (red) and truncated Xklp1$_{506}$–GFP (black) and parabolic fits (dashed lines, see Experimental Procedures). Error bars are SEM.

(G) Histograms of the initial brightness of Xklp1–GFP, Xklp1$_{506}$–GFP, and dimeric Kin$_{401}$–GFP as a control (Telley et al., 2009), indicating that both fragment and full-length Xklp1 are dimeric.

See also Figure S4 and Movie S7.

directional switches of ∼2.3 s and a velocity of ∼0.5 μm/s for Xklp1 in the overlap. For time intervals larger than the persistence time, the movement of Xklp1 was effectively diffusive.

To estimate which distances Xklp1 can explore in PRC1-decorated antiparallel microtubule overlaps, we calculated the distribution of average exploratory distances (Figure 6D, black dots, Extended Experimental Procedures). This analysis reveals that Xklp1 can explore average lengths of up to ∼6 μm. This is in strong contrast to the low exploratory distances of PRC1 (Figure 6D, blue dots), which can only move for distances of up to ∼0.2 μm. Strikingly, the average exploratory distances of individual Xklp1 molecules coincide well with the range of steady-state lengths of antiparallel microtubule overlaps (Figure 4B). This suggests that, by processive movement, Xklp1 reaches the plus ends of antiparallel overlapping microtubules, where it can modulate microtubule dynamics. To test whether the processive nature of Xklp1's motility is indeed central to the mechanism of steady-state length establishment, we replaced adenosine-5′-triphosphate (ATP) by adenosine-5′-diphosphate (ADP) in the TIRF microscopy experiment, thereby preventing processive motility of Xklp1 but not its recruitment by PRC1. We observed that under these conditions the two midzone proteins failed to produce stable steady-state overlap lengths (Figure S6). Instead, overlap microtubules continued growing despite the presence of PRC1 and Xklp1 in the overlap. We conclude that processive overlap exploration allows Xklp1 to reach and modulate the behavior of microtubule plus ends and that its finite

average exploratory range limits the maximum size of the steady-state antiparallel microtubule overlap length to 5–6 μm (Figure 4B, Figure 6D). This defines a processive exploration mechanism for antiparallel microtubule overlap length control.

## DISCUSSION

### The Mechanism of Antiparallel Overlap Generation and Length Control by PRC1/Kinesin-4 Explains Anaphase Spindle Characteristics In Vivo

We have elucidated a molecular mechanism capable of selective formation and adaptable length control of antiparallel microtubule overlaps by two conserved midzone proteins. Central to this mechanism is the combination of four distinct molecular activities (Figure 7): (1) bundling of microtubules with high selectivity for antiparallel orientation by PRC1, (2) recruitment of kinesin-4 by PRC1 to antiparallel overlaps, and (3) processive microtubule plus-end-directed motility together with (4) an inhibitory effect on microtubule growth by the motor protein kinesin-4. The combination of these activities constitutes a minimal two-component system capable of formation of a minimal midzone in vitro.

Our in vitro reconstitution explains why loss of either PRC1 or kinesin-4 leads to nonequivalent defects in midzone formation in vivo (Kurasawa et al., 2004; Mollinari et al., 2002; Zhu and Jiang, 2005). We show that selective antiparallel microtubule crosslinking is an intrinsic property of vertebrate PRC1, an activity which appears to be evolutionarily conserved (Janson
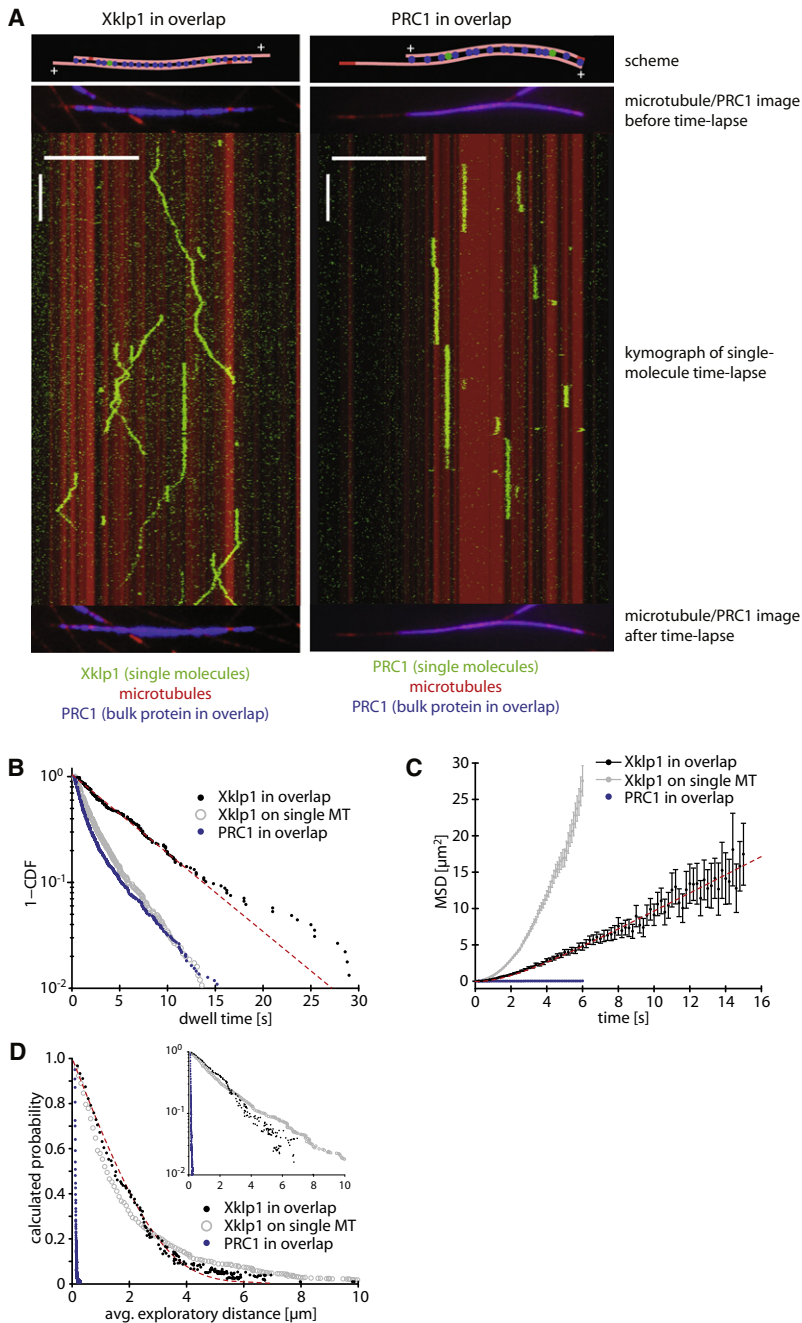
**Figure 6. Xklp1 Determines Antiparallel Microtubule Overlap Length by Processive Overlap Exploration**

(A) Single-molecule imaging of either individual Xklp1–GFP molecules (500 pM, green) in a PRC1–Alexa 647 (5 nM, blue) containing antiparallel microtubule overlap (red) (right panel) or individual PRC1–Alexa 647 molecules (5 pM, green) in a PRC1–Alexa 488 (5 nM, blue) containing antiparallel microtubule overlap (red) (left panel). Scheme (top) and triple-channel TIRF microscopy images of the microtubule pair before (upper image) and after (lower image) fast time-lapse imaging of individual Xklp1–GFP or PRC1–Alexa 647 molecules, as illustrated in a kymograph (middle). The frame rate was 10 s$^{-1}$. Horizontal scale bar, 10 μm. Vertical scale bar, 5 s.

(B) Dwell time distribution (shown as 1 − CDF) of single Xklp1–GFP molecules moving in antiparallel microtubule overlap regions (conditions as in A, right; black dots, n = 226) and a monoexponential fit (dashed red); mean dwell time is 5.85 ± 0.12 s (mean ± 95% CI). For comparison, the distributions for Xklp1–GFP on single taxol-microtubules (gray circles, under conditions as in Figure 5B) and for PRC1–Alexa 647 in a PRC1–Alexa 488-containing antiparallel overlap (blue dots, under conditions as in A, left) are shown.

(C) Mean squared displacement (MSD) curves for the same conditions as shown in (B), and a fit to the data of Xklp1–GFP in antiparallel overlaps using the "persistent random walk" model, yielding persistence time $T_p$ = 2.31 ± 0.68 s and mean velocity $v$ = 0.52 ± 0.06 μm/s (mean ± 95% CI, see Experimental Procedures). Error bars are SEM.

(D) Calculated probability distribution of the average exploratory distance (black dots, see Extended Experimental Procedures) of Xklp1–GFP molecules in antiparallel overlaps and the predicted probability curve (dashed red) calculated from the persistent random walk model using the parameter values as obtained from the fits in (B) and (C). For comparison, calculated average exploratory distance distributions are plotted for Xklp1–GFP on single stabilized microtubules and PRC1–Alexa 647 in overlaps (as in B and C). Inset: semi-logarithmic plot of average exploratory distances.

See also Figure S5, Figure S6, and Movie S8.

et al., 2007). Autonomous bundling of antiparallel microtubules places PRC1 at the core of the activities essential for midzone formation and explains why PRC1 is absolutely required for the bundling and stabilization of antiparallel microtubule overlaps, as indicated by the complete loss of central anaphasic microtubule bundles in the absence of PRC1 in vivo (Kurasawa et al., 2004; Mollinari et al., 2002; Zhu and Jiang, 2005).

Vertebrate PRC1 has previously been shown to interact with kinesin-4 during anaphase, an interaction necessary for proper midzone organization (Kurasawa et al., 2004; Zhu and Jiang, 2005). Here, we establish a hierarchy of interactions: full-length

*Xenopus* kinesin-4 Xklp1 binds only weakly to microtubules. However, by interacting with PRC1, Xklp1 is recruited to antiparallel microtubule overlaps, reminiscent of selective recruitment of sliding motors of the kinesin-5 and kinesin-6 families by Ase1 in budding yeast and fission yeast, respectively (Fu et al., 2009; Khmelinskii et al., 2009). This recruitment results in the local inhibition of microtubule plus-end growth in antiparallel overlaps by Xklp1, leading to a defined steady-state overlap length. This explains why the midzone unnaturally extends but half-spindles remain connected upon loss of kinesin-4 in vivo, resulting in long, distorted anaphase spindles (Kurasawa et al., 2004; Zhu and Jiang, 2005).

**Processive Overlap Exploration by Kinesin-4 Ensures Adaptive Overlap Length Control**

Xklp1 reduces the dynamicity of microtubules by lowering the turnover of tubulin at the growing microtubule end. On individual
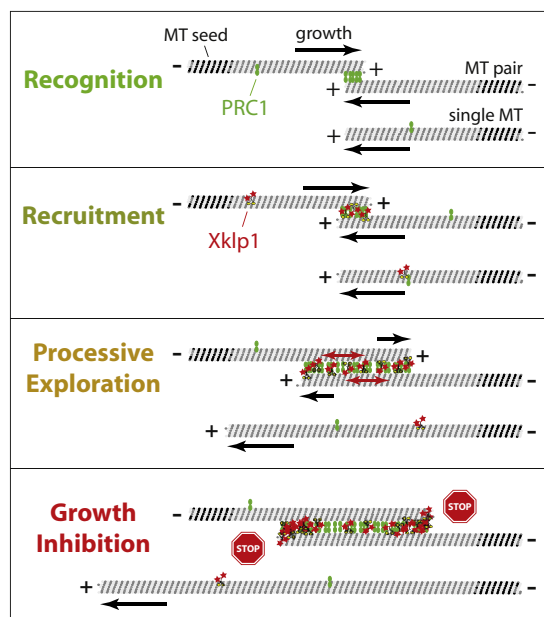
**Figure 7. A Two-Component System Controls Antiparallel Microtubule Overlaps**

Model illustrating schematically the activities that lead in their combination to antiparallel microtubule overlap formation and length control (see Discussion).

microtubules this activity can be observed in vitro only at highly elevated Xklp1 concentrations (several hundred nanomolar) well above physiological levels (Bieling et al., 2010a). In contrast, recruitment of Xklp1 to antiparallel microtubule overlaps by PRC1 results in complete inhibition of microtubule growth already at lower, close-to physiological concentrations at which individual microtubules remain unaffected in their growth. As a consequence, specific recruitment of Xklp1 ensures the local inhibition of growth of only those microtubules engaged in antiparallel, PRC1-decorated microtubule overlaps. Activation of the PRC1/kinesin-4 system, through dephosphorylation at anaphase onset, therefore results in tight bundling and growth inhibition of antiparallel microtubule overlaps in the central spindle (Kurasawa et al., 2004; Mollinari et al., 2002; Zhu and Jiang, 2005), whereas microtubules residing outside of the midzone are likely not affected by the PRC1/kinesin-4 system.

Xklp1 motors move processively with velocities of around 0.5 μm/s within the PRC1-decorated antiparallel microtubule overlap (Figure 6C, Figure S5B). The drag force exerted by PRC1 on Xklp1 can be estimated to be low (Extended Experimental Procedures) compared to typical stall forces of kinesins (Carter and Cross, 2005; Svoboda and Block, 1994), explaining why Xklp1 is slowed down only mildly by interacting with PRC1. This explains why Xklp1 efficiently explores the antiparallel overlap instead of generating substantial microtubule sliding forces. This contrasts Xklp1 to antiparallel microtubule sliding motors like kinesin-5, which reside relatively static between the sliding microtubules (Kapitein et al., 2005; Kapoor and Mitchison, 2001; Miyamoto et al., 2004; Uteng et al., 2008).

How does processive movement of Xklp1 within the antiparallel overlap region result in length control? Accumulation of

Xklp1 at growing microtubule ends (Figure 5A) is likely to be responsible for the dose-dependent inhibition of microtubule growth (Figure 4). The targeting of Xklp1 to growing microtubule ends is reminiscent of the manner by which the microtubule depolymerizing kinesins Kip3 (kinesin-8) (Varga et al., 2006, 2009) and MCAK (kinesin-13) (Helenius et al., 2006) reach the ends of artificially stabilized microtubules. Both proteins are "collected" from an extended region near the end of stabilized microtubules in vitro either by directional (Kip3) or diffusive (MCAK) motility. Xklp1 (kinesin-4) is also collected from an extended region, however, in this case from the microtubule overlap by processive bidirectional motility (Figure 6A, Figure S5A). For such an "antenna mechanism" to be effective under conditions where microtubules grow, it is important that the velocity of Xklp1 in the overlap (~0.5 μm/s [Figure 6C, Figure S5B]) is considerably faster than the velocity with which the microtubules elongate (~35 nm/s in our in vitro experiments and ~200 nm/s in vivo [Rusan et al., 2001; Tournebize et al., 1997]). This might explain why Xklp1 is a fast motor in comparison to other mitotic kinesins.

The lowest Xklp1 concentration (5 nM) required to form antiparallel microtubule overlaps with stable steady-state lengths resulted in overlaps of around 5 μm (Figure 4B). This length is in remarkably good agreement with the maximal exploratory distance of individual Xklp1 molecules in PRC1-enriched antiparallel overlaps (Figure 6D). This suggests that the threshold amount of Xklp1 required to induce a complete stop of microtubule growth is reached at this concentration by exploiting the entire exploratory range of Xklp1 molecules in the overlap. At higher concentrations, the threshold amount is already reached by "collecting" from shorter overlaps, leading to characteristic overlap lengths as a function of the Xklp1 concentration. In *Xenopus* egg extract, the concentration of Xklp1 is approximately 100 nM (Bieling et al., 2010a). Our experiments predict that such concentrations lead to overlap lengths of ~2 μm (Figure 4B), which is in agreement with a midzone length of 2–3 μm as measured in vivo (Kurasawa et al., 2004; Mastronarde et al., 1993; Zhu and Jiang, 2005).

The PRC1/kinesin-4 system offers adaptive, self-regulatory control of overlap size by introducing a negative feedback between overlap length and microtubule growth. Shortening the microtubule overlaps as a consequence of motor-driven microtubule sliding would result in lowered amounts of kinesin-4 at the microtubule ends because the motor could be collected now only from shorter distances. Similar to our reversibility experiment where we reduced the global concentration of Xklp1 (Figures 4C–4E), the system would be predicted to dynamically respond to antiparallel sliding resulting in shortening overlaps by initiating microtubule elongation. Local, selective inhibition of microtubule growth by kinesin-4 in antiparallel overlaps at conditions that globally favor microtubule elongation therefore allows for a dynamic control of overlap length.

## Antiparallel Microtubule Overlaps in Yeasts and Metazoans

Maintenance of stable antiparallel microtubule overlaps in the spindle center requires coordination between microtubule (de)polymerization and microtubule sliding. In particular, spindle elongation during anaphase B must not compromise spindle stability by potentially reducing the length of the antiparallel

overlap region. Several proposals have been made for mechanisms to locally regulate microtubule dynamics in the anaphase spindle (Cheerambathur et al., 2007; Gardner et al., 2008; Pearson et al., 2006). Interestingly, recent work in fission yeast has linked the conserved microtubule-binding protein CLASP to the stabilization of antiparallel microtubule bundles (Bratman and Chang, 2007). Ase1-dependent recruitment of CLASP to antiparallel microtubule overlaps has been suggested to prevent microtubule depolymerization past the overlap by inducing microtubule rescue (Bratman and Chang, 2007). A similar PRC1-dependent stabilizing function of CLASP for antiparallel microtubule overlaps during anaphase appears also to exist in cultured human cells (Liu et al., 2009).

Although local induction of microtubule rescue might explain how overlap stability is ensured, it does not readily explain how microtubule overgrowth is prevented and thus how a defined overlap size is established. This is especially the case for metazoan systems in which microtubule growth velocities are high (Kinoshita et al., 2001). Our in vitro experiments have demonstrated how the PRC1/kinesin-4 system can control antiparallel overlap length at conditions that globally favor microtubule elongation. It might be the combination of inhibition of microtubule growth by kinesin-4 and the promotion of rescues by CLASP that ensures the stabilization and length control of antiparallel microtubule overlaps in metazoans. The adaptive nature of this mechanism would allow for independent regulation of antiparallel microtubule sliding activities at different stages of anaphase.

In contrast to metazoan anaphase spindles, the length of antiparallel microtubule overlaps does not appear to be tightly controlled in yeast. Microtubule plus ends are dynamic in fission yeast anaphase spindles as well as in bundled interphase arrays (Sagolla et al., 2003). The slower microtubule growth velocities in yeast might be one reason for less stringent control of the overlap size in this organism. In addition, yeast uses the processive motor kinesin-8 (Klp5/6 in fission yeast and Kip3 in budding yeast) as the major microtubule plus-end-destabilizing factor (Cottingham et al., 1999; Gupta et al., 2006; West et al., 2001). Length-dependent destabilization of microtubules by kinesin-8 (Tischer et al., 2009; Varga et al., 2006) might be sufficient for a less stringent control of overlap stability. This might explain the absence of kinesin-4 from both fission and budding yeast.

During interphase, fission yeast also uses antiparallel microtubule overlaps as means to organize the microtubule cytoskeleton. Recently, a model for the formation of such overlaps was proposed based on the combined action of the sliding motor Klp2 (a kinesin-14) and Ase1 (Janson et al., 2007). In this model, antiparallel microtubules slide with respect to each other driven by minus-end-directed motors targeted selectively to microtubule plus ends. Sliding stops either as a consequence of plus ends growing beyond the overlap region or possibly by friction exerted by overlap-enriched Ase1 (Janson et al., 2007). This leads to the formation of antiparallel microtubule overlaps with inverted polarity and dynamically varying sizes, a mechanism that differs from that of tight overlap size control during metazoan anaphase.

## Conclusion

We have reconstituted a two-component system necessary and sufficient to form antiparallel microtubule overlaps with precisely defined length in vitro, an essential process for proper midzone formation in metazoan anaphase spindles. The in vitro reconstitution allowed us to dissect the mechanism of autonomous antiparallel microtubule recognition by PRC1 and of local microtubule growth inhibition and overlap length control by kinesin-4. In the future, the extension of our reconstitution approach by including other midzone proteins promises to yield further mechanistic understanding of aspects of the organization and function of the late mitotic spindle.

## EXPERIMENTAL PROCEDURES

### Dynamic Microtubule Overlap Assay

A flow chamber assembled from a biotin-PEG functionalized glass coverslip and a PLL-PEG passivated glass slide separated by two stripes of double-sided tape (Bieling et al., 2010b) was filled with a series of solutions: (1) Pluronic F-127 and $\kappa$-casein, (2) NeutrAvidin and $\kappa$-casein, (3) buffer, (4) short GMP–CPP stabilized, biotinylated brightly labeled microtubule seeds (containing 26% Alexa Fluor 568-labeled tubulin), (5) buffer. Microtubule growth was initiated by flowing in dimly labeled tubulin (containing 10% Alexa Fluor 568-labeled tubulin) together with midzone proteins at the indicated concentrations. The final assay buffer was 80 mM K-PIPES, pH 6.8, 85 mM KCl, 85 mM K-acetate, 4 mM MgCl$_2$, 1 mM GTP, 2 mM MgATP, 1 mM EGTA, 10 mM $\beta$-mercaptoethanol, 0.25% [wt/wt] Brij-35, 0.1% methyl cellulose, 100 $\mu$g/ml $\beta$-casein, and oxygen scavengers. If not stated otherwise, the concentrations of proteins were 5 nM PRC1–Alexa 647, 15 nM Xklp1–GFP or Xklp1$_{506}$–GFP, and 17.5 $\mu$M dimly labeled tubulin.

To test the reversibility of antiparallel microtubule overlap formation, overlaps were allowed to form in the presence of 5 nM PRC1–Alexa 647, 100 nM Xklp1–GFP (PRC1:Xklp1 ratio of 1:20), and 17.5 $\mu$M dimly labeled tubulin for 7–10 min at 28°C ± 1°C. Then the PRC1:Xklp1 ratio was changed to 1:1 by flowing in a solution with only 5 nM Xklp1–GFP, leaving all other concentrations constant.

Multicolor time-lapse imaging using TIRF microscopy was always performed at 28°C ± 1°C.

### Single-Molecule Imaging

Single full-length Xklp1–GFP molecules were imaged at a concentration of 2.5 nM on individual paclitaxel-stabilized, biotinylated, and fluorescently labeled microtubules (5% Alexa 568-labeled tubulin) in low ionic strength buffer (80 mM K-PIPES, pH 6.8, 85 mM K-acetate, 4 mM MgCl$_2$, 2 mM MgATP, 1 mM EGTA, 10 mM $\beta$-mercaptoethanol, 10 $\mu$M paclitaxel, 0.25% [wt/wt] Brij-35, 100 $\mu$g/ml $\beta$-casein, and oxygen scavengers). Xklp1$_{506}$–GFP at 20 nM, or Kin$_{401}$–GFP at 0.1 nM as a control, was imaged in very low ionic strength buffer (12 mM K-PIPES, pH 6.8, 2 mM MgCl$_2$, 2 mM MgATP, 1 mM EGTA, 10 mM $\beta$-mercaptoethanol, 10 $\mu$M paclitaxel, 100 $\mu$g/ml $\beta$-casein, and oxygen scavengers).

For imaging individual PRC1–Alexa 647 molecules in dynamic antiparallel microtubule overlaps, the PRC1–Alexa 647 concentration was lowered to 50 pM or to 5 pM in the presence of 5 nM PRC1–Alexa 488. For imaging individual Xklp1–GFP molecules in dynamic, PRC1-containing antiparallel microtubule overlaps, the Xklp1–GFP concentration was lowered to 500 pM.

### Data Analysis

The movements of single fluorescent molecules were analyzed using automated particle tracking (Kalaimoscope, TransInsight, Dresden, Germany) (Telley et al., 2009). For dwell time distributions, the cumulative distribution function (CDF) of data was calculated using the "ecdf" function in Matlab (MathWorks), and either a monoexponential or a biexponential function was fitted to (1–CDF) data using a "least-squares" approach. Histograms of run lengths were fitted with a monoexponential function as described (Telley et al., 2009). MSD curves were calculated and fitted using the function $v^2 \Delta t^2 + 2D \Delta t$ + offset, with the mean velocity $v$ and the diffusion coefficient $D$. For the case of Xklp1 in the overlap the MSD curve was fitted to a "persistent random walk" model (Othmer et al., 1988; Tranquillo and Lauffenburger,

1987): MSD = $2v^2T_p[\Delta t - T_p(1 - \exp(-\Delta t/T_p))]$ with the persistence time $T_p$ and mean velocity $v$, and hence $v^2T_p$ the effective diffusion coefficient. The "average exploratory distance" distribution in microtubule overlaps was calculated by combining information from the dwell time distribution and the MSD curve in antiparallel microtubule overlaps, thereby eliminating time. Microtubule dynamics was determined by kymograph analysis using ImageJ. The growth versus tubulin concentration relationship in the presence or absence of Xklp1 was analyzed using a multiple linear regression model with a categorical factor $g$ (+Xklp1: $g = 0$, –Xklp1: $g = 1$) and $y = b_1 + m_1 x + g$ ($b_2 + m_2 x$). Generally, this analysis provides a significance test for differences in the slope $m$ and abscissa $b$ of two linear relationships. Here, the slope and abscissa represent the kinetic parameters $k_{on}$ and $-k_{off}$, respectively, of the microtubule dynamics.

## SUPPLEMENTAL INFORMATION

Supplemental Information includes Extended Experimental Procedures, six figures, and eight movies and can be found with this article online at doi:10.1016/j.cell.2010.06.033.

## REFERENCES

Arnal, I., Heichette, C., Diamantopoulos, G.S., and Chretien, D. (2004). CLIP-170/tubulin-curved oligomers coassemble at microtubule ends and promote rescues. Curr. Biol. 14, 2086–2095.

Bieling, P., Kronja, I., and Surrey, T. (2010a). Microtubule motility on reconstituted meiotic chromatin. Curr. Biol. 20, 763–769.

Bieling, P., Telley, I.A., Hentrich, C., Piehler, J., and Surrey, T. (2010b). Fluorescence microscopy assays on chemically functionalized surfaces for quantitative imaging of microtubule, motor, and +TIP dynamics. Methods Cell Biol. 95, 555–580.

Bratman, S.V., and Chang, F. (2007). Stabilization of overlapping microtubules by fission yeast CLASP. Dev. Cell 13, 812–827.

Bringmann, H., Skiniotis, G., Spilker, A., Kandels-Lewis, S., Vernos, I., and Surrey, T. (2004). A kinesin-like motor inhibits microtubule dynamic instability. Science 303, 1519–1522.

Brouhard, G.J., Stear, J.H., Noetzel, T.L., Al-Bassam, J., Kinoshita, K., Harrison, S.C., Howard, J., and Hyman, A.A. (2008). XMAP215 is a processive microtubule polymerase. Cell 132, 79–88.

Carter, N.J., and Cross, R.A. (2005). Mechanics of the kinesin step. Nature 435, 308–312.

Cheerambathur, D.K., Civelekoglu-Scholey, G., Brust-Mascher, I., Sommi, P., Mogilner, A., and Scholey, J.M. (2007). Quantitative analysis of an anaphase B switch: predicted role for a microtubule catastrophe gradient. J. Cell Biol. 177, 995–1004.

Cottingham, F.R., Gheber, L., Miller, D.L., and Hoyt, M.A. (1999). Novel roles for saccharomyces cerevisiae mitotic spindle motors. J. Cell Biol. 147, 335–350.

Drechsel, D.N., Hyman, A.A., Cobb, M.H., and Kirschner, M.W. (1992). Modulation of the dynamic instability of tubulin assembly by the microtubule-associated protein tau. Mol. Biol. Cell 3, 1141–1154.

Fu, C., Ward, J.J., Loiodice, I., Velve-Casquillas, G., Nedelec, F.J., and Tran, P.T. (2009). Phospho-regulated interaction between kinesin-6 Klp9p and microtubule bundler Ase1p promotes spindle elongation. Dev. Cell 17, 257–267.

Gardner, M.K., Bouck, D.C., Paliulis, L.V., Meehl, J.B., O'Toole, E.T., Haase, J., Soubry, A., Joglekar, A.P., Winey, M., Salmon, E.D., et al. (2008). Chromosome congression by Kinesin-5 motor-mediated disassembly of longer kinetochore microtubules. Cell 135, 894–906.

Glotzer, M. (2009). The 3Ms of central spindle assembly: microtubules, motors and MAPs. Nat. Rev. Mol. Cell Biol. 10, 9–20.

Gupta, M.L., Jr., Carvalho, P., Roof, D.M., and Pellman, D. (2006). Plus end-specific depolymerase activity of Kip3, a kinesin-8 protein, explains its role in positioning the yeast mitotic spindle. Nat. Cell Biol. 8, 913–923.

Helenius, J., Brouhard, G., Kalaidzidis, Y., Diez, S., and Howard, J. (2006). The depolymerizing kinesin MCAK uses lattice diffusion to rapidly target microtubule ends. Nature 441, 115–119.

Howard, J., and Hyman, A.A. (2007). Microtubule polymerases and depolymerases. Curr. Opin. Cell Biol. 19, 31–35.

Janson, M.E., de Dood, M.E., and Dogterom, M. (2003). Dynamic instability of microtubules is regulated by force. J. Cell Biol. 161, 1029–1034.

Janson, M.E., Loughlin, R., Loiodice, I., Fu, C., Brunner, D., Nedelec, F.J., and Tran, P.T. (2007). Crosslinkers and motors organize dynamic microtubules to form stable bipolar arrays in fission yeast. Cell 128, 357–368.

Jiang, W., Jimenez, G., Wells, N.J., Hope, T.J., Wahl, G.M., Hunter, T., and Fukunaga, R. (1998). PRC1: A human mitotic spindle-associated CDK substrate protein required for cytokinesis. Mol. Cell 2, 877–885.

Kapitein, L.C., Peterman, E.J., Kwok, B.H., Kim, J.H., Kapoor, T.M., and Schmidt, C.F. (2005). The bipolar mitotic kinesin Eg5 moves on both microtubules that it crosslinks. Nature 435, 114–118.

Kapitein, L.C., Janson, M.E., van den Wildenberg, S.M., Hoogenraad, C.C., Schmidt, C.F., and Peterman, E.J. (2008). Microtubule-driven multimerization recruits ase1p onto overlapping microtubules. Curr. Biol. 18, 1713–1717.

Kapoor, T.M., and Mitchison, T.J. (2001). Eg5 is static in bipolar spindles relative to tubulin: evidence for a static spindle matrix. J. Cell Biol. 154, 1125–1133.

Khmelinskii, A., and Schiebel, E. (2008). Assembling the spindle midzone in the right place at the right time. Cell Cycle 7, 283–286.

Khmelinskii, A., Lawrence, C., Roostalu, J., and Schiebel, E. (2007). Cdc14-regulated midzone assembly controls anaphase B. J. Cell Biol. 177, 981–993.

Khmelinskii, A., Roostalu, J., Roque, H., Antony, C., and Schiebel, E. (2009). Phosphorylation-dependent protein interactions at the spindle midzone mediate cell cycle regulation of spindle elongation. Dev. Cell 17, 244–256.

Kinoshita, K., Arnal, I., Desai, A., Drechsel, D.N., and Hyman, A.A. (2001). Reconstitution of physiological microtubule dynamics using purified components. Science 294, 1340–1343.

Kurasawa, Y., Earnshaw, W.C., Mochizuki, Y., Dohmae, N., and Todokoro, K. (2004). Essential roles of KIF4 and its binding partner PRC1 in organized central spindle midzone formation. EMBO J. 23, 3237–3248.

Kwon, M., Morales-Mulia, S., Brust-Mascher, I., Rogers, G.C., Sharp, D.J., and Scholey, J.M. (2004). The chromokinesin, KLP3A, dives mitotic spindle pole separation during prometaphase and anaphase and facilitates chromatid motility. Mol. Biol. Cell 15, 219–233.

Lee, Y.M., and Kim, W. (2004). Kinesin superfamily protein member 4 (KIF4) is localized to midzone and midbody in dividing cells. Exp. Mol. Med. 36, 93–97.

Liu, J., Wang, Z., Jiang, K., Zhang, L., Zhao, L., Hua, S., Yan, F., Yang, Y., Wang, D., Fu, C., et al. (2009). PRC1 cooperates with CLASP1 to organize central spindle plasticity in mitosis. J. Biol. Chem. 284, 23059–23071.

Loiodice, I., Staub, J., Setty, T.G., Nguyen, N.P., Paoletti, A., and Tran, P.T. (2005). Ase1p organizes antiparallel microtubule arrays during interphase and mitosis in fission yeast. Mol. Biol. Cell 16, 1756–1768.

Mastronarde, D.N., McDonald, K.L., Ding, R., and McIntosh, J.R. (1993). Interpolar spindle microtubules in PTK cells. J. Cell Biol. *123*, 1475–1489.

Miyamoto, D.T., Perlman, Z.E., Burbank, K.S., Groen, A.C., and Mitchison, T.J. (2004). The kinesin Eg5 drives poleward microtubule flux in Xenopus laevis egg extract spindles. J. Cell Biol. *167*, 813–818.

Mollinari, C., Kleman, J.P., Jiang, W., Schoehn, G., Hunter, T., and Margolis, R.L. (2002). PRC1 is a microtubule binding and bundling protein essential to maintain the mitotic spindle midzone. J. Cell Biol. *157*, 1175–1186.

Muller, S., Smertenko, A., Wagner, V., Heinrich, M., Hussey, P.J., and Hauser, M.T. (2004). The plant microtubule-associated protein AtMAP65-3/PLE is essential for cytokinetic phragmoplast function. Curr. Biol. *14*, 412–417.

Othmer, H.G., Dunbar, S.R., and Alt, W. (1988). Models of dispersal in biological systems. J. Math. Biol. *26*, 263–298.

Pearson, C.G., Gardner, M.K., Paliulis, L.V., Salmon, E.D., Odde, D.J., and Bloom, K. (2006). Measuring nanometer scale gradients in spindle microtubule dynamics using model convolution microscopy. Mol. Biol. Cell *17*, 4069–4079.

Powers, J., Rose, D.J., Saunders, A., Dunkelbarger, S., Strome, S., and Saxton, W.M. (2004). Loss of KLP-19 polar ejection force causes misorientation and missegregation of holocentric chromosomes. J. Cell Biol. *166*, 991–1001.

Rusan, N.M., Fagerstrom, C.J., Yvon, A.M., and Wadsworth, P. (2001). Cell cycle-dependent changes in microtubule dynamics in living cells expressing green fluorescent protein-alpha tubulin. Mol. Biol. Cell *12*, 971–980.

Sagolla, M.J., Uzawa, S., and Cande, W.Z. (2003). Individual microtubule dynamics contribute to the function of mitotic and cytoplasmic arrays in fission yeast. J. Cell Sci. *116*, 4891–4903.

Schuyler, S.C., Liu, J.Y., and Pellman, D. (2003). The molecular function of Ase1p: evidence for a MAP-dependent midzone-specific spindle matrix. Microtubule-associated proteins. J. Cell Biol. *160*, 517–528.

Svoboda, K., and Block, S.M. (1994). Force and velocity measured for single kinesin molecules. Cell *77*, 773–784.

Telley, I.A., Bieling, P., and Surrey, T. (2009). Obstacles on the microtubule reduce the processivity of Kinesin-1 in a minimal in vitro system and in cell extract. Biophys. J. *96*, 3341–3353.

Tischer, C., Brunner, D., and Dogterom, M. (2009). Force- and kinesin-8-dependent effects in the spatial regulation of fission yeast microtubule dynamics. Mol. Syst. Biol. *5*, 250.

Tournebize, R., Andersen, S.S., Verde, F., Doree, M., Karsenti, E., and Hyman, A.A. (1997). Distinct roles of PP1 and PP2A-like phosphatases in control of microtubule dynamics during mitosis. EMBO J. *16*, 5537–5549.

Tranquillo, R.T., and Lauffenburger, D.A. (1987). Stochastic model of leukocyte chemosensory movement. J. Math. Biol. *25*, 229–262.

Uteng, M., Hentrich, C., Miura, K., Bieling, P., and Surrey, T. (2008). Poleward transport of Eg5 by dynein-dynactin in Xenopus laevis egg extract spindles. J. Cell Biol. *182*, 715–726.

Varga, V., Helenius, J., Tanaka, K., Hyman, A.A., Tanaka, T.U., and Howard, J. (2006). Yeast kinesin-8 depolymerizes microtubules in a length-dependent manner. Nat. Cell Biol. *8*, 957–962.

Varga, V., Leduc, C., Bormuth, V., Diez, S., and Howard, J. (2009). Kinesin-8 motors act cooperatively to mediate length-dependent microtubule depolymerization. Cell *138*, 1174–1183.

Verbrugghe, K.J., and White, J.G. (2004). SPD-1 is required for the formation of the spindle midzone but is not essential for the completion of cytokinesis in *C. elegans* embryos. Curr. Biol. *14*, 1755–1760.

Verni, F., Somma, M.P., Gunsalus, K.C., Bonaccorsi, S., Belloni, G., Goldberg, M.L., and Gatti, M. (2004). Feo, the *Drosophila* homolog of PRC1, is required for central-spindle formation and cytokinesis. Curr. Biol. *14*, 1569–1575.

Vernos, I., Raats, J., Hirano, T., Heasman, J., Karsenti, E., and Wylie, C. (1995). Xklp1, a chromosomal *Xenopus* kinesin-like protein essential for spindle organization and chromosome positioning. Cell *81*, 117–127.

Walczak, C.E., and Heald, R. (2008). Mechanisms of mitotic spindle assembly and function. Int. Rev. Cytol. *265*, 111–158.

Walker, R.A., O'Brien, E.T., Pryer, N.K., Soboeiro, M.F., Voter, W.A., Erickson, H.P., and Salmon, E.D. (1988). Dynamic instability of individual microtubules analyzed by video light microscopy: rate constants and transition frequencies. J. Cell Biol. *107*, 1437–1448.

West, R.R., Malmstrom, T., Troxell, C.L., and McIntosh, J.R. (2001). Two related kinesins, klp5+ and klp6+, foster microtubule disassembly and are required for meiosis in fission yeast. Mol. Biol. Cell *12*, 3919–3932.

Zhu, C., and Jiang, W. (2005). Cell cycle-dependent translocation of PRC1 on the spindle by Kif4 is essential for midzone formation and cytokinesis. Proc. Natl. Acad. Sci. USA *102*, 343–348.

Zhu, C., Zhao, J., Bibikova, M., Leverson, J.D., Bossy-Wetzel, E., Fan, J.B., Abraham, R.T., and Jiang, W. (2005). Functional analysis of human microtubule-based motor proteins, the kinesins and dyneins, in mitosis/cytokinesis using RNA interference. Mol. Biol. Cell *16*, 3187–3199.

**Note Added in Proof**

In a manuscript by Subramanian et al., which appears in this issue of *Cell*, the authors arrive at similar conclusions regarding the nature of microtubule cross-links formed by PRC1.